UC Berkeley
UC Berkeley Previously Published Works

Title

Moisture self-regulating ionic skins with ultra-long ambient stability for self-healing energy and sensing systems

Permalink

https://escholarship.org/uc/item/99x551d9

Authors

He, Peisheng
Long, Yu
Fang, Chao
et al.

Publication Date

2024-09-01

DOI

10.1016/j.nanoen.2024.109858

Peer reviewed

eScholarship.org Powered by the California Digital Library
University of California

Moisture Self-Regulating Ionic Skins with Ultra-Long Ambient Stability for Self-Healing Energy and Sensing Systems

Peisheng He [a,†], Yu Long [a,†], Chao Fang [b,†], Christine Heera Ahn [a], Ashley Lee [a], Chun-Ming Chen [a], Jong Ha Park [a], Monong Wang [c], Sujoy Kumar Ghosh [a], Wenying Qiu [a], Ruiqi Guo [a], Renxiao Xu [a], Zhichun Shao [a], Yande Peng [a], Likun Zhang [a], Baoxia Mi [c], Junwen Zhong [a,d,*] and Liwei Lin [a,*]

[a] Department of Mechanical Engineering & Berkeley Sensor & Actuator Center, University of California Berkeley, Berkeley, California, 94720, USA.

[b] Sustainable Energy and Environment Thrust, Function Hub, The Hong Kong University of Science and Technology (Guangzhou), Nansha, Guangzhou, 511400, Guangdong, China.

[c] Department of Civil and Environmental Engineering, University of California Berkeley, Berkeley, California, 94720, USA.

[d] Department of Electromechanical Engineering and Centre for Artificial Intelligence and Robotics, University of Macau, Macau SAR, 999078, China.

[*] Correspondence to: junwenzhong@um.edu.mo, lwlin@berkeley.edu

Abstract: Dehydration has been a key limiting factor for the operation of conductive hydrogels in practical application. Here, we report self-healable ionic skins that can self-regulate their internal moisture level by capturing extenral moistures via hygroscopic ion-coordinated polymer backbones through antipolyelectrolyte effect. Results show the ionic skin can maintain its mechanical and electrical functions over 16 months in the ambient environment with high stretchability (fracture stretch ~2216%) and conductivity (23.5 mS/cm). The moisture self-regulating capability is further demonstrated by repeated exposures to harsh environments such as 200°C heating, freezing, and vacuum drying with recovered conductivity and stretchability. Their reversible ionic and hydrogen bonds also enable self-healing feature as a sample with the fully cut-through damage can restore its conductivity after 24 h at 40% relative humidity. Utilizing the ionic skin as a building block, self-healing flexible piezoelecret sensors have been constructed to monitor physiological signals. Together with a facile transfer-printing process, a self-powered sensing system with a self-healable supercapacitor and humidity sensor has been successfully demonstrated. These results illustrate broad-ranging possibilities for the ionic skins in applications such as energy storage, wearable sensors, and human-machine interfaces.

Keywords: Hydrogels, Self-powered sensor, Ionic skins, Ambient stability, Self-healing

Introduction

Self-healing materials that are stretchable and ionically conductive have great potentials in flexible electronics such as electrolytes in batteries[1–3] and supercapacitors[4–7], as well as electrodes in ionotronic devices[8–12]. Among various self-healing material systems[13–19], hydrogels show good promise by combining high ion conductivity, high stretchability, and good self-healing properties, but they generally suffer from the long-term stability issue due to the dehydration process. For instance, polyacrylamide hydrogels can dry out within several hours under the ambient air[9,20] and previously reported self-healable hydrogels without encapsulation suffer from the same dehydration problem such that they can only work under high humidity conditions[4,5,15,21,22]. To enhance the ambient stability, many additives have been incorporated into the polymer network to form various ion-conducting gels. For example, ionogels consist of polymer networks swollen by non-volatile ionic liquids[12,23,24] but most ionogels are toxic and expensive with non-ideal ionic conductivity[25–28] . Alcohols, such as ethylene glycol and glycerol, have been investigated as the anti-dehydration additives[6,7,29–32] to form organogel or organohydrogel. However, the increased viscosity results in the reduction in their electrical conductivity[15,29,33–35]. Alcohol also exhibits low but non-negligible vapor pressure and could evaporate together with water molecules in water-alcohol mixtures[36,37] , which degrades their long-term and healing stability. On the other hand, hydrogels with added hygroscopic salt have been shown to adsorb moisture at low humidity for applications in atmospheric water harvesting systems[38–40]. However, excessive swelling is reported in these systems, impairing the mechanical properties and self-healing ability[20,41–43]. Moreover, phase instabilities such as salt leakage and agglomeration are often observed as a result of the salting-out effect[44,45]. As such,

a grand challenge of self-healing conductive material for soft electronics is a stable system to sustain long-term operations with high stretchability and good ionic conductivity in the ambient environment for practical applications.

In this work, highly deliquescent salt is controllably loaded to zwitterionic-based polymer backbone for highly stretchable ionic skins to simultaneously achieve: (1) self-regulation of internal moisture for long-lasting stability; and (2) self-healing from severe mechanical damages (such as a through cut) in the ambient. The moisture adsorption capability is greatly enhanced by the dissociated hygroscopic salt ions that coordinates with the zwitterionic backbone via the anti-polyelectrolyte effect[46]**.** Specifically, hygroscopic salt ions are adsorbed to oppositely charged cationic and anionic functional groups thus screening self-association of zwitterionic polymer chains (**Fig. 1a**). These "locked" salt ions then in turn form adsorptive centers to bond water molecules through salt hydration. The high concentration salt can be stably and homogeneously incorporated without inducing phase separation due to mutually cohesive interactions among water, ions, and polymer backbone. In synergy with the ionic and hydrogen-bonds provided by the polymer backbone, the hydrogel can effectively capture water molecules through the salt hydration and/or bonding with the polymer backbone to achieve the self-regulation of water content via the absorbing/desorbing process in the ambient air. To realize the self-healing property, moieties with hydrogen-bond donors are introduced on the polymer backbone to form reversible crosslinks such as hydrogen bonds and ionic interactions with the zwitterionic moieties. The reversible reconstruction of these multiple sets of dynamic bonds enables their self-healing capability. Experimental results show that water content can be replenished to maintain several key properties such as transparency, conductivity, and stretchability with little degradation in the ambient air for

over 16 months (**Fig. 1b**, **Fig. S1** and **S2**). This is the longest storage period (**Fig. 1c** and **Table S1**) ever reported for stretchable ionic conductors in the literature. Furthermore, the hydrogels have shown high stretchability (maximum fracture stretch ~2216%), ion conductivity (23.5 mS/cm), and the ability to repeatedly recover from exposures to harsh conditions such as high temperature (200 °C), low temperature (-20 °C), and vacuum (hundreds of mTorr) while maintaining it self-healing property (**Fig. 1d** and **Fig. S1**). Prototype devices such as a self-healable soft piezoelecret sensor, printed micro-supercapacitors and humidity sensors, have been fabricated and tested as key demonstrations examples toward practical applications.

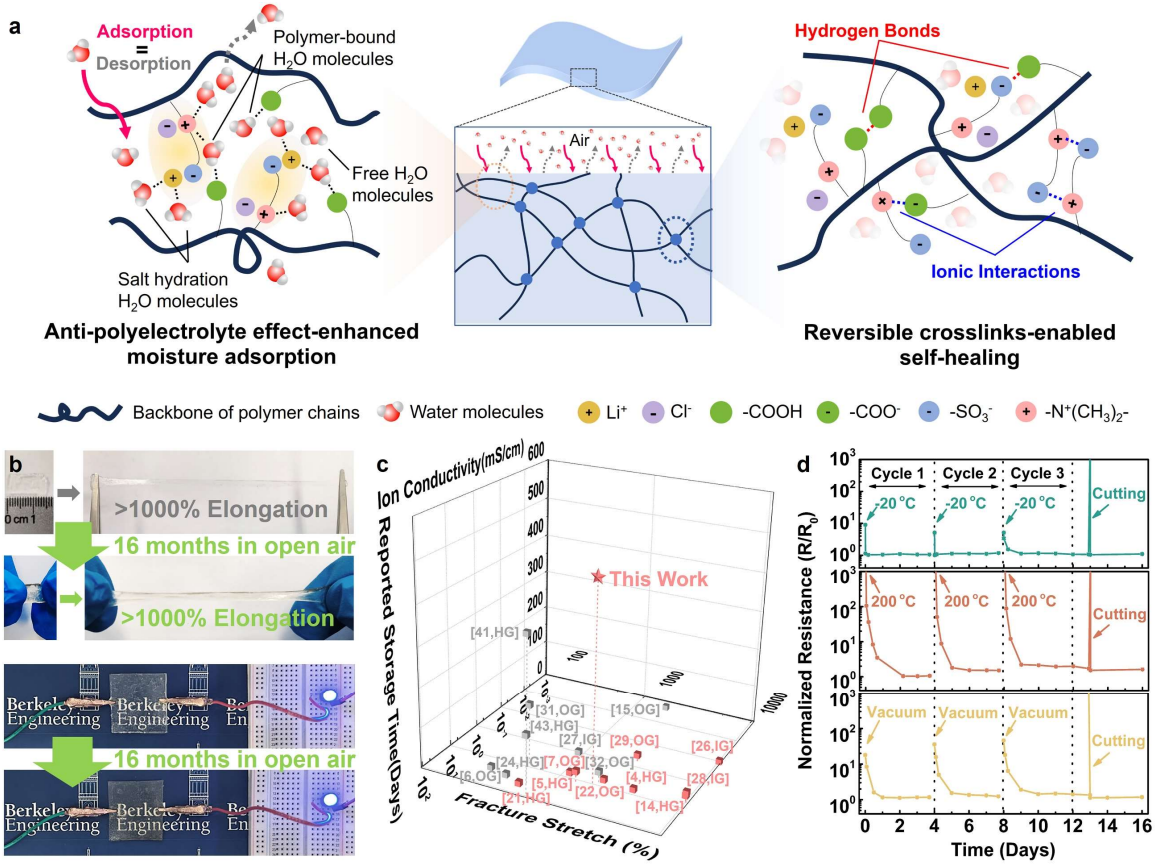

Fig. 1. Molecular design and properties of moisture self-regulating self-healable ionic skin. (a) Conceptual illustration of the water self-regulation and self-healing mechanism. Left: moisture

self-regulation mechanism. Hygroscopic salt ions are dissociated by zwitterionic moieties via the anti-polyelectrolyte effect, forming adsorptive centers to capture water molecules through salt hydration and/or bonding with polymer backbones. Right: the reversible crosslinks such as ionic interactions and hydrogen bonds between polymer chains to enable the self-healing process. **(b)** the transparent hydrogel-based ionic skin maintains high stretchability (>1000% elongation, top figures) and good ionic conductivity after over 16 months in the ambient air (bottom figures). **(c)** Comparison of ionic skins in terms of fracture stretch, ionic conductivity, and storage time (red: self-healable; grey: non-self-healable). HG: hydrogel; OG: organohydrogel or organogel; IG: ionogel. **(d)** Normalized resistance changes of MA-LiCl hydrogels with respect to time during three consecutive recovery cycles in the ambient air with a relative humidity (RH) of 50% after exposures to low temperature of -20 ℃ for 1 day (green), high temperature of 200 ℃ for 30 mins (red), and vacuum of hundreds of mTorr for 16 h (yellow), respectively. All samples are subjected to a through-cut process by a razor blade after three cycles and subsequently reconnected. The resistance changes before cutting, after the self-healing process for one minute, and 3 days are recorded.

Results and discussion

Water retention and self-regulation

The proposed hydrogel is synthesized by a simple one-pot random copolymerization of 2-(methacryloyloxy)ethyl)dimethyl-(3-sulfopropyl) ammonium hydroxide (MEDSAH) as zwitterionic monomer and acrylic acid (AA) for the hydrogen-bond donor in the LiCl solution by using N,N'-methylenebisacrylamide (MBAA) as the covalent crosslinker (**Fig. S3**). The resulting poly(MEDSAH-co-AA)/LiCl hydrogel is denoted as MA-LiCl hydrogel for simplicity. It is well known that the addition of non-volatile solute such as salt could lead to the reduction of the solvent vapor pressure[47,48]. However, a substantial reduction of the water vapor pressure in the hydrogel could be required to reach an equilibrium with the ambient air and a high salt concentration might be needed for good ion conductivity. As such, a large amount of solute must be incorporated into the solution, which can easily lead to the salt crystallization and/or phase separation. Therefore, salts with a high solubility in water and strong attraction to both water and polymer backbone are desirable. LiCl is selected due to its strong interaction with water molecules, exhibiting high solubility (~25 moles of LiCl per kilogram of water) and deliquescence behavior at a relative low humidity of 11.3%[48] with high water adsorption uptake (reaching ~2.6 g g^{-1} at RH 60%)[49]. The effective dissociation of salt in the hydrogel system is realized by the incorporation of zwitterionic monomer MEDSAH, whose anti-polyelectrolyte effect enhances salt-polymer backbone affinity through charge-charge interactions. Plain MA hydrogels and MA hydrogels incorporated with the same concentration (4 M in precursor solution) of NaCl, and ethylene glycol (EG) are also synthesized (denoted as MA, MA-NaCl, and MA-EG, respectively) and studied for comparison.

To evaluate the water retention capability of these hydrogels, their ion conductivities and total mass retention ratios under different humidity conditions are recorded over 7 days (**Fig. S4** and **S5**) and their equilibrated values are plotted in **Fig. 2a** and **b**, respectively. The resulting MA-LiCl hydrogel shows the best water retention capability under various humidity levels. Specifically, it exhibits a conductivity of 0.0034 mS/cm when the relative humidity drops to 17%. Meanwhile, no appreciable change in mass of MA-LiCl hydrogels is observed after 7 days (**Fig. S6**) from relative humidity (RH) of 75% down to RH 17%, suggesting that the water uptake of the hydrogel is capable of reaching equilibrium within the tested humidity range. In contrast, plain MA hydrogels and MA-NaCl hydrogels lose their electrical conductivities at RH 69% and RH 28% within 24 h, respectively due to the dehydration process. This is also confirmed by the thermogravimetric analysis (TGA) as shown in **Fig. S7**, where plain MA and MA-NaCl hydrogels show significant weight losses upon heating at ~100 ℃. Additionally, the salt-induced freeze-point depression effect[50] results in the excellent anti-freezing property of the MA-LiCl hydrogel down to -80 ℃ as revealed by the differential scanning calorimetry (DSC) spectra in **Fig. S8**.

Recently, alcohol-based (glycerol, ethylene glycol, … *etc.*) organohydrogels or organogels have been reported to show good water-retention capabilities[6,7,29–32,51]. Compared with the MA-LiCl hydrogel, the as synthesized MA-EG hydrogel exhibits similar water retention behavior and anti-freezing properties (**Fig. S7 and S8**). However, the MA-EG hydrogel has lower ionic conductivities and loses its ion conductivity at RH 28% after 3 days (**Fig. S4)**. Interestingly, the MA-EG hydrogel at RH 69% loses its conductivity completely when stored over an extended period (~ 6 months) due to the non-negligible volatility of EG, while the MA-LiCl hydrogel still has ~90% of the original conductivity after 16 months (**Fig. S2**) as water can be replenished from

the moisture in the air. It is worth noting that these tests are discontinued when this paper is written and an even longer storage time is expected.

Humidity tends to fluctuate in the actual ambient environment. In order to further study the moisture self-regulation process in changing ambient humidities, a cyclic test has been performed. Hydrogels are subjected periodically to dry (RH 17%, 5 days) and humid (RH 69%, 5 days) environments in an alternating fashion. **Fig. S9** depicts the conductivity changes of different hydrogels over one cycle. It is found that the plain MA hydrogel loses its conductivity even in a relatively high humid condition of RH 69%. After the 5-day exposure in the dry condition, MA-NaCl and MA-EG hydrogels lose their conductivity, while the MA-LiCl hydrogel has 3 orders of magnitude reduction in its conductivity. MA-LiCl hydrogel recovers most of its original conductivity in one day and almost fully recovers its original conductivity in 4 days after placed back in the RH 69% environment. A total of 6 cycles have been conducted and results are plotted in **Fig. 2c**. The conductivity of MA-EG hydrogel shows a gradual decay and becomes unmeasurable after 5 cycles due to the evaporation of ethylene glycol over time. Such phenomenon is more evident when MA-EG hydrogels are exposed to incidental heating or vacuum conditions as the evaporation of EG is expedited. Specifically, **Fig. S10** shows that the MA-EG hydrogel can only recover ~30% of its conductivity after the overnight vacuum drying process and loses it conductivity after heated at 200 ℃ for 30 min. In comparison, the conductivity of MA-LiCl shows excellent recovery ability after multiple cycles of drastic humidity changes during the period of over 2 months (**Fig. 2c**). As such, MA-LiCl samples are able to deliver consistent conductivity once being placed to an environment with the original relative humidity even after being stored over 16 months in ambient air with various environmental fluctuations (**Fig. S2**). The stretchability of the

MA-LiCl hydrogel is also maintained over the extended storage period (**Fig. S1**). It should be noted the tensile strength of the material decreased due to the prolonged exposure to sunlight. The extended *uv* irradiation from sunlight exposure leads to the decrease in the MBAA covalent crosslinking[52,53] and result in a mechanical behavior similar to those observed for MA-LiCl hydrogel without MBAA crosslinker (**Fig. S11**) or MBAA-crosslinked hydrogel after the 200 ℃ heating process (**Fig. S1**).

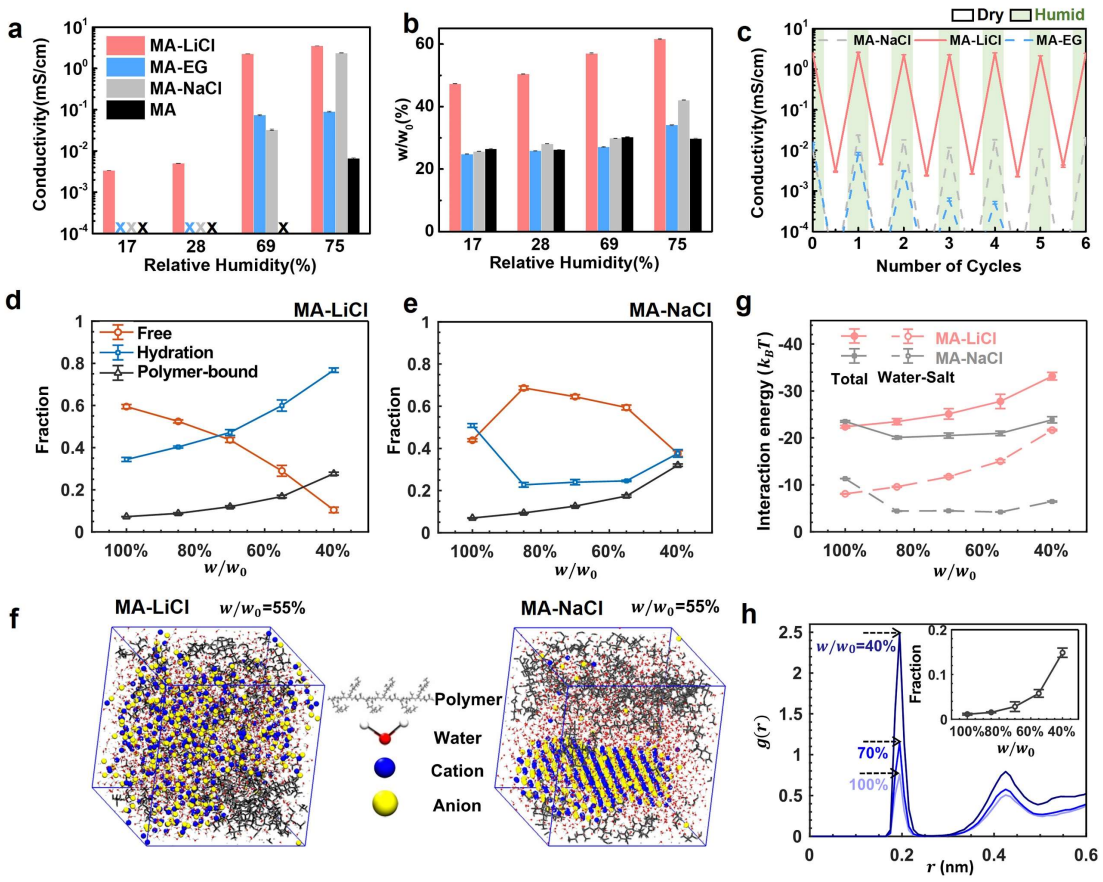

Fig. 2. Water retention and self-regulation. (a) Ionic conductivity, and **(b)** total mass retention ratio w/w_0 measured at equilibrium states after 7 days of storage at each relative humidity for the plain MA hydrogels and hydrogels with different anti-dehydration additives. The total mass retention ratio w/w_0 is obtained by normalizing the final mass of each sample to their initial mass. Prior to the experiment, all samples are stored and equilibrated at RH 80%. The concentrations of

all additives in precursor solutions are kept at 4 mol/L. **(c)** Ionic conductivity of hydrogels with different anti-dehydration additives over 6 moisture self-regeneration cycles, where samples are placed in alternating humidity chambers of RH 69% for 5 days and RH 17% for 5 days, repeatedly. MD simulation results showing the fractional variation of free water, hydration water, and polymer-bound water with respect to the overall water content: **(d)** MA-LiCl hydrogel, and **(e)** MA-NaCl hydrogel. **(f)** Snapshots of MA-LiCl hydrogel (left) and MA-NaCl hydrogel system (right) when both systems are about 55% of their initial mass (w/w_0= 55%). **(g)** Average interaction energy of a single water molecule: with the whole system (filled symbols) and with the salt (open symbols) in MA-LiCl hydrogel (red circles) and MA-NaCl hydrogel system (grey squares). **(h)** Radial distribution function of Li^+ ions around the $-SO_3^-$ and carboxylate groups of polymer backbone in the MA-LiCl hydrogel. The inset shows the fraction of water molecules that serve simultaneously as hydration water and polymer-bound water.

To investigate the origin of the strong water retention and self-regulation behavior of MA-LiCl hydrogel, molecular dynamics (MD) simulations have been performed for the water-ion-zwitterionic polymer ternary system. In pure hydrogel (water-polymer) binary systems, elucidation of water interactions is commonly realized by inspecting the states of water molecules based on the hydrogen bonding with polymer chains [54–57] . Here, the states of water are defined as: (1) “polymer-bound water” that forms hydrogen bonds with polymer, (2) “hydration water” that is within the first solvation shell of ions, and (3) the remaining “free water” that does not directly interact with polymer chains or ions. The system is taken to be in equilibrium when the number of water molecules in each state stabilizes (**Fig. S12**). **Fig. 2d** shows that as the total water content

reduces (w/w_0 <100%), the fraction of free water drops dramatically in the MA-LiCl hydrogel whereas those of polymer-bound and hydration water increase. This implies that the water evaporation process in the MA-LiCl hydrogel is dominated by the reduction of the free water, reminiscent of that in pure hydrogel systems[58] . **Fig. 2e** shows the states of water in the MA-NaCl hydrogel. By contrast, the fraction of free water increases initially at w/w_0 =85% and drops afterwards while the fraction of hydration water drops initially at w/w_0 =85% and increases afterwards. These results are attributed to the much lower solubility of NaCl in water than that of LiCl due to weak water-ion interactions (**Fig. S13**)[47,59]. As further revealed by snapshots of MD simulations (**Fig. 2f**), LiCl is homogenously dispersed even at a low water content (w/w_0 =55%), while the majority of NaCl has precipitated into crystals. As the domains of NaCl crystals formed, fewer Na^+ and Cl^- could participate in the interaction with water molecules, yielding an increased fraction of free water. This facilitates the evaporation process, and in turn leads to more NaCl aggregations. Such positive feedback mechanism ultimately leads to the macroscopic crystallization and drying out of hydrogel as observed in experiments (**Fig. S14**). The disparate states of water in the two hydrogels are manifested for more stabilized water in the MA-LiCl hydrogel. In particular, **Fig. 2g** shows that the average interaction energy of a single water molecule is stronger in the MA-LiCl hydrogel than those in the MA-NaCl hydrogel, which is mainly caused by interactions with salt ions. Overall, the superior solubility of LiCl in water gives rise to the large fraction of stabilized hydration water, which enables the high retention of water in MA-LiCl hydrogel.

In addition to water molecules, the interaction between ions and polymer backbone is examined from the pair distribution function for Li^+ around the negatively charged moieties of the zwitterionic

polymer, *i.e.*, $-SO_3^-$ and carboxylate groups. As shown in **Fig. 2h**, the peak height increases significantly at reducing water content, suggesting a stronger binding between ions and polymer chains as evaporation proceeds. This result is in line with the increasing overlap of polymer-bound and hydration water at lower water content (**Fig. 2h inset**), which suggests an increasing number of water molecules are shared between the salt and polymer backbone. Such mutually cohesive water-ion-polymer interactions will benefit the dissociation of LiCl at low humidity, which further augments the solubility in hydrogel and thereby enhances water retention.

Meanwhile, simulation results of the MA-EG hydrogel system show low interaction between water and EG (**Fig. S15**), which is consistent with the similar water loss ratio of MA-EG hydrogel and MA-NaCl hydrogel (**Fig. 2b**). Unlike salt-hydrogel systems, as water evaporates, EG can serve as a solvent in the system to promote ion transports and chain movements even in the absence of water. This gives rise to the finite conductivity of MA-EG hydrogel at low humidity conditions as shown in **Fig. 2a and 2c**.

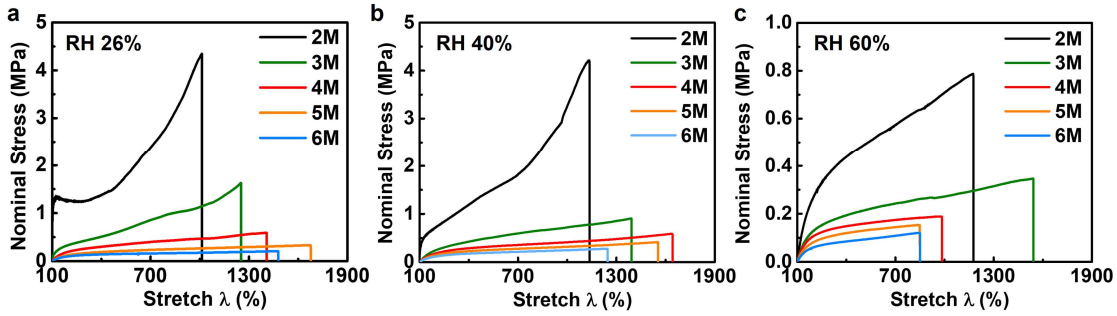

Fig. 3. Stress-stretch curves of MA-LiCl hydrogels with different initial LiCl concentrations in the precursor solutions under different relative humidity levels. (a) RH 26%, **(b)** RH 40%, and **(c)** RH 60%. The stretch λ, is defined as the ratio of the distance between two clamps during the stretching process divided by their initial distance. The MBAA content is fixed at 0.03% for all tests and the stretch rate is kept at 2 min^{-1}.

By exploiting the absorption/desorption equilibrium between LiCl and ambient moisture, water content within the hydrogel at a given relative humidity can be tuned by incorporating different amount of LiCl into the MA-LiCl hydrogel for a wide spectrum of electrical (**Fig. S16**) and mechanical properties. **Fig. 3** shows the stress-stretch curve of MA-LiCl hydrogels with different concentrations (2 M to 6 M) of LiCl in precursor solutions (crosslinker mol% fixed at 0.03%) under different relative humidity levels (26%, 40%, and 60%). At a low humidity level such as RH 26% shown in **Fig. 3a**, the mechanical properties of MA-LiCl are mainly limited by low water content that impedes the polymer chain movements. As such, increasing the LiCl concentration can increase the moisture adsorption and thus significantly lower the modulus (from ~21 MPa for 2 M down to ~0.24 MPa for 6 M) as well as the tensile strength (from ~4.3 MPa for 2 M LiCl down to ~0.21 MPa for 6 M LiCl). On the other hand, the stretchability increases (fracture stretch from 1013% for 2 M LiCl to 1675% for 5 M LiCl). At elevated humidity or salt concentration, the excessive water content can lead to swelling, and cause the pre-stretching[60] of the polymer network to result in reduced stretchability. Therefore, stretchability of MA-LiCl hydrogel starts to peak at around 5 M at RH 26% with a fracture stretch of 1675% (**Fig. 3a**), 4 M at RH 40% with a fracture stretch 1639% (**Fig. 3b**), and 3 M at around RH 60% with a fracture stretch of 1541% (**Fig. 3c**). Despite the wide range of modulus, within tested humidity range of RH 26% - 60%, all MA-LiCl hydrogels are able to reach stretches of over 800% before fracture and a maximum fracture stretch of ~2216% can be attained (**Fig. S11**). The formation of dynamic crosslinking network could account for the overall high stretchability in the broad range of humidity levels. During the mechanical stretching process, multiple physical crosslinks detach and relax the polymer chains, thereby dissipating the mechanical energy of the network [61,62].

Autonomous self-healing in the ambient environment

A proposed mechanism for self-healing of the MA-LiCl hydrogel is shown in **Fig. 4a**, which can be generally attributed to two steps. In the first step, the dynamic bonds reform at the wounded surfaces when they are brought into physical contacts as exemplified in the snapshots of MD simulations. The backbone of co-polymerized MEDSAH and AA provides multiple sets of dynamic bonds, including ionic associations between $-COO^-$ and quaternary ammonium groups, $-SO_3^-$ and quaternary ammonium groups, as well as hydrogen bonds between hydrogen donors (-COOH) and acceptors ($-SO_3^-$ and ester carbonyl groups). To illustrate the contribution of hydrogen bonds in the self-healing process, a hydrogel sample is first incised with a razor blade and reconnected to allow the reformation of dynamic bonds for one minute. Subsequently, urea solution is applied on the cutting area, which is known to disrupt hydrogen bonds[4,63]. As shown in **Fig. S17**, the self-healed hydrogel was able to support a mass of ~200 g initially. It fractured rapidly along the original cutting interfaces within 5 s upon urea coating, while in control experiment, another healed hydrogel under same condition still sustains the mass 10 minutes after the coating of DI water. The reversible hydrogen bonds and ionic interactions are further characterized by the horizontal attenuated total reflectance-Fourier transform infrared spectroscopy (HATR-FTIR) spectra (**Fig. S18**) and Raman spectroscopy (**Fig. S19**). The C=O stretching vibration band of poly(acrylic acid)/LiCl hydrogel (PAA-LiCl) is located at a low wavenumber of ~1711 cm^{-1} while that of the control hydrogel sample consisting of only zwitterionic MEDSAH backbone (PMEDSAH-LiCl) is located at 1722 cm^{-1} which corresponds to the free ester carbonyl groups[26,64]. In MA-LiCl hydrogel, the corresponding vibration band shifts to 1719 cm^{-1}, which can be attributed the formation of hydrogen bonds between hydrogen-bond donors and acceptors. S=O stretching

vibration of $-SO_3^-$ group in MA-LiCl hydrogel exhibits a significant blueshift both in FTIR (from 1039 to 1046 cm^{-1}) and Raman (from 1041 to 1045 cm^{-1}) spectra compared to that in PMEDSAH-LiCl. This indicates electrostatic ionic interactions between the positively and negatively charged functional groups[65,66]. Once dynamic bonds reform, a network of ion-transporting channels is established, and the ion-conductivity of the hydrogel could recover in a short period of time. As shown in **Fig. 4b**, the hydrogel is cut in halves by a razor blade and the two halves are attached together to allow the healing process in the ambient environment. Within one minute, over 90% of its conductivity is recovered. A total of twenty cutting-and-healing cycles are performed at the same location on the hydrogel and over 90% of the conductivity is recovered in each test as attributed to the reformation of reversible dynamic bonds for the repeatable self-healing capability. In the second step, after the instant reformation of dynamic bonds, polymer chains also migrate across the wounded interface *via* interdiffusion to further strengthen the healed interface. This agrees well with observations during the tensile tests on healed hydrogel samples (**Fig. 4c inset**), where wounded surfaces have merged with restored mechanical integrity. In addition, the mechanical properties of healed hydrogels recover gradually (**Fig. S20**), indicative of a time-dependent interdiffusion process.

Water content in hydrogel plays a key role in the self-healing performance of MA-LiCl. A series of tensile tests are performed or both pristine and self-healed (for 24 h at room temperature) MA-LiCl hydrogels with different LiCl concentrations (2 M to 6 M, crosslinker concentration is fixed at 0.03%) under a range of relative humidity (RH 26% to 60%). Herein stretchability recovery rate is calculated by dividing the fracture strain of a self-healed specimen by that of the pristine specimen. As shown in **Fig. S21**, at low humidity such as RH 26%, the self-healing performance

is mainly restricted by low chain mobility that impedes the polymer chain movement across the wounded interface. As such, an increase in the stretchability recovery rate is observed when LiCl concentration rises from 2 M to 3 M as LiCl can absorb moistures. It is noted that the self-healing performance at the elevated humidity or high salt concentration experiences a reduction, which could result from excessive water content that causes swelling. Meanwhile, the role of crosslinker content is also studied by tensile tests for MA-LiCl hydrogels by varying MBAA concentration as compared to monomers (**Fig. S22**). Interestingly, the covalent crosslinking cannot reconstruct after damages, but at low crosslinker concentration, the self-healing performance is found to initially increase with high crosslinker content until a peak is reached at 0.01% (**Fig. S22b**) for MA-LiCl hydrogel (4 M LiCl in precursor solution) at RH 40%. This increase could be attributed to the fact that the increase in crosslinker concentration reduces the water uptake of the hydrogel [67]. Therefore, the swelling of hydrogel is alleviated and thus a stretchability recovery of ~100% can be reached for self-healed MA-LiCl hydrogel (4 M LiCl, 0.01% MBAA) at RH 40% as shown in **Fig. 4c**. After the healing process, the wounded area is healed almost completely as observed by scanning electron microscopy (SEM) in **Fig. 4d**. However, further increasing the crosslinker concentration introduces excessive amount of unrecoverable covalent crosslinking content to result in a decrease in the self-healing efficiency.

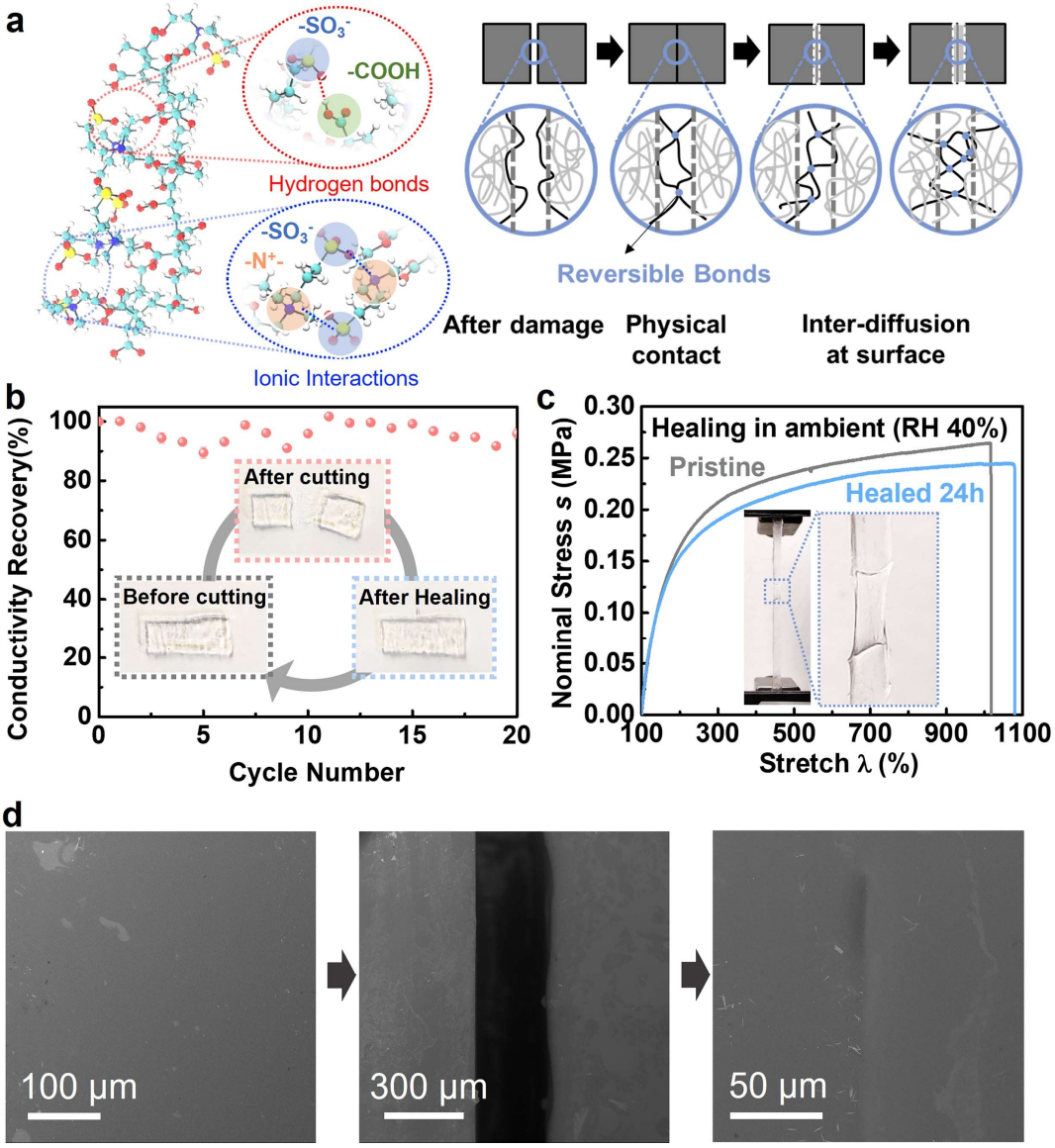

Fig. 4. Self-healing of hydrogel. (a) Left: a snapshot from the MD simulation depicting reversible bonds. Color code for atoms: hydrogen in white, carbon in cyan, nitrogen in blue, oxygen in red, and sulfur in yellow. Right: the schematic illustration of the two-step self-healing process, including the instantaneous reformation of reversible bonds at damaged surfaces and subsequent interdiffusions of polymer chains across the interface. **(b)** Conductivity recovery of MA-LiCl hydrogel (4 M LiCl, 0.06% MBAA) after each cutting-healing cycle. The healing time for each cycle is one minute. Inset: digital photos showing the hydrogel before cutting, after cutting and

after healing. **(c)** Stress-stretch curves of pristine and self-healed (under RH 40% at room temperature for 24 h) MA-LiCl hydrogel (4 M LiCl, 0.01% MBAA). Inset: Optical image of a healed hydrogel during a tensile test. Right inset figure: enlarged view of the optical image showing the healed area in the tensile test process. **(d)** SEM images showing the hydrogel before cutting, after cutting, and after healing in the ambient environment for 24 h.

Self-healing flexible piezoelectret sensor

Since the stretching of the hydrogel mostly induces changes on conformation of polymer chains and water molecules, it has negligible effects on the material ion conductivity[12]. It is found that when stretched λ times of its initial length, the resistance of the hydrogel, R, scales approximately as: $R=R_0\lambda^2$ (R_0 is the initial resistance) up to a large 700% stretch in **Fig. S23**. Compared to the stretchable electron-conducting conductors in published reports [68–70], which are often based on conductive percolating paths, the electro-mechanical performance of hydrogel in this work exhibits better stability and predictability under a large strain. Besides, the hydrogel also shows excellent transparency (**Fig. S24**). With a thick strip of 1 mm, a transmittance of over 82.5% is observed across the visible spectrum (400-700 nm).

These attributes, combined with the excellent ambient stability and self-healing ability, make MA-LiCl hydrogel potentially suitable as stretchable transparent electrodes in human-machine interface systems. As a proof-of-concept, a self-healing flexible and transparent piezoelectret sensor with MA-LiCl hydrogel electrodes has been demonstrated as shown in **Fig. 5a**. Herein we used MA-LiCl hydrogels with 4 M LiCl for fabrication of device as they demonstrated good stretchability under our lab ambient humidity (RH 40%~50%). The elastic modulus of the hydrogel

is ~200 kPa, which is comparable to that of human epidermis (140 to 600 kPa)[2]. The hydrogel top electrode is packaged between the top elastomer layer of VHB (Very High Bond, 3M) and top fluorinated ethylene propylene (FEP) layer. This prevents the direct contact of MA-LiCl to human skin to prevent the potential skin irritation or salt loss due to the natural perspiration of human body. FEP is used as the electret material due to its outstanding ability to capture and retain surplus electrostatic charges[71]. Air gaps are formed between two FEP films separated by a VHB spacer layer with hole openings. A corona charging process is performed to polarize FEP films thereby forming megascopic electrical dipoles inside the air gaps. The compression and release of the device lead to changes in the distance of the air gap and the electrostatic field to convert mechanical movements into electrical signals as illustrated in **Fig. S25**. **Fig. 5b** shows that the sensor is attached to the human arm to monitor muscle movements from various gestures. The contraction/relaxation of muscle movements are transduced into corresponding current signals, while the magnitude of the gesture is captured by the amplitude of the current as shown in **Fig. 5c** and **Video 1**. The same hydrogel has been used as electrodes as prepared and after 30 days of exposure in ambient air, with both devices exhibiting similar performances without degradations. To further evaluate the continuous operation stability, the output current of the prototype sensor is measured when stimulated with a cyclic applied normal pressure of 22.5 kPa at 1 Hz for over 1000 cycles. As shown in **Fig. S26**, the time waveform of the output current from the sensor remains stable, demonstrating the good repeatability of the ionic skin-based piezoelecret sensor. By exploiting the self-healing ability of hydrogel and VHB[72], it is demonstrated that the piezoelectret sensor can recover from a through cut by a razor blade after self-healing process in the ambient for 24 h (**Fig. S27**). Muscle contraction/relaxation signals measured on the same volunteer with the healed sensor

shows similar responses as compared to those measured by the pristine device (**Fig. 5d**). Additionally, the prototype sensor can also be used to monitor pulses (**Fig. S28**) and collected data are shown in **Fig. 5e**, where delicate waveforms with clear characteristics of systolic peaks, points of inflection and dicrotic waves can be clearly distinguished.

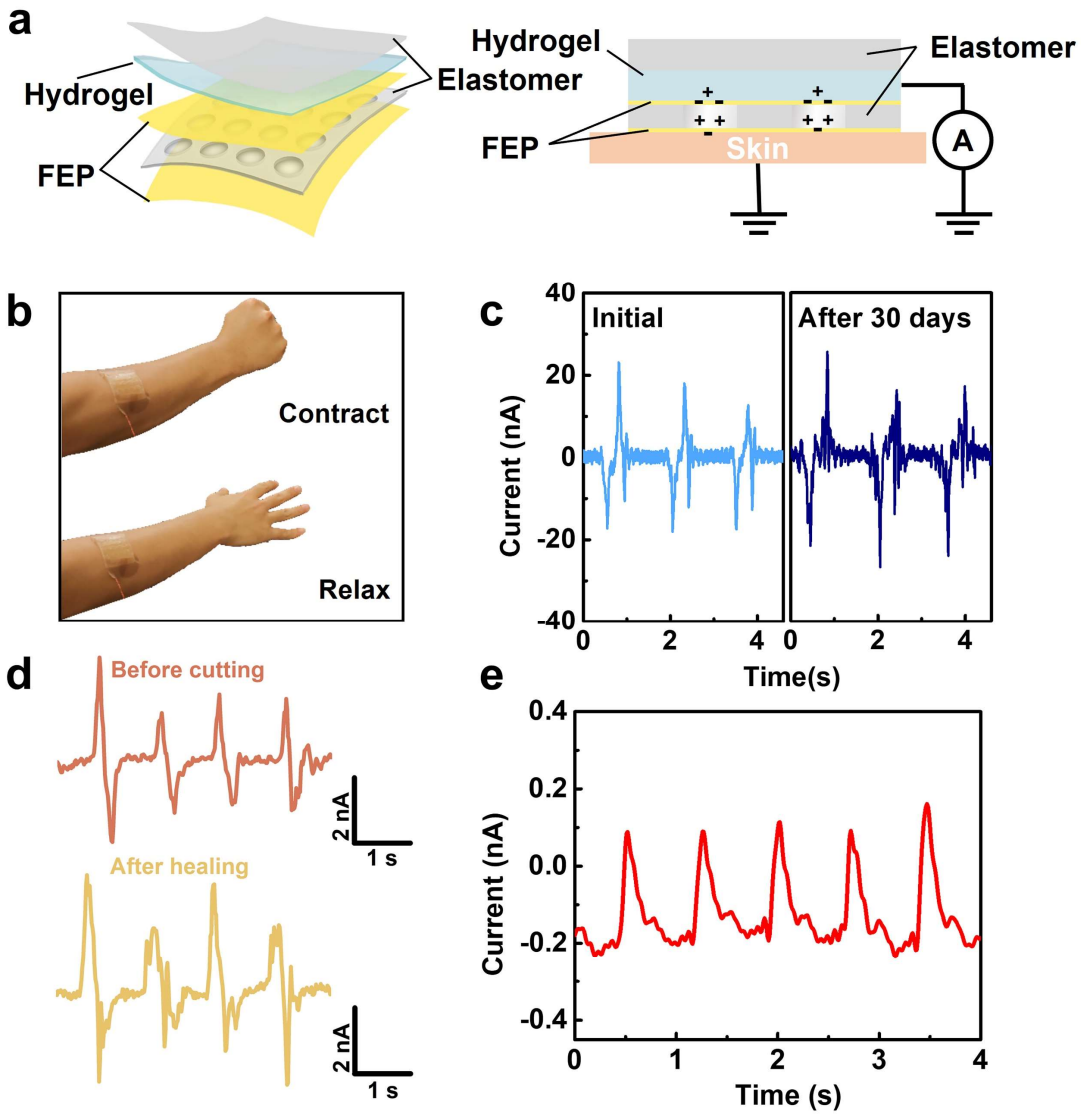

Fig. 5. Self-healing and self-powered flexible piezoelectret sensor. (a) Left: the sensor structure. Right, the cross-sectional view of the sensor illustrating the sensing mechanism. **(b)** A prototype sensor to monitor muscle contraction/relaxation. **(c)** The corresponding current responses before

(left) and after 30-day (right) storage in the ambient air. **(d)** Muscle contraction/relaxation signals by the piezoelectric sensor captured before and after the throught cut with a razor blade and subsequent self-healing process in the ambient for 24 h. **(e)** Pulse signals measured from a prototype sensor.

Patterning on ionic skins

Due to the abundant hydrogen bonds in the ionic skin, the material is self-adhesive and can adhere to a variety of substrate materials such as glass and plastic (**Fig. S29**). Here, a transfer-printing process is developed to allow the patterning of different materials onto the hydrogel film with good resolutions. First, thin-film materials are first patterned on a different substrate using processes such as photolithography, screen printing and others. Second, the patterned material layer is peeled off and transferred onto the hydrogel film. As a demonstration example, specific patterns made of carbon nanotubes are constructed and transferred on the hydrogel substrate as a sensing system with a self-healable supercapacitor and humidity sensor (**Fig. 6a**). In this process, a 50 μm-thick polyethylene terephthalate (PET) film is applied on top of a filter paper to form a bilayer structure. A vinyl cutter is utilized to cut the upper PET film and unwanted parts are peeled off to define designed electrode patterns[73]. Carbon nanotubes (CNTs) dispersed in an aqueous solution are filtered with the masked filter paper and the remaining PET structures are removed. Next, the filter paper with CNT patterns on top is flipped and pressed on top of an MA-LiCl hydrogel substrate. The strong adhesion from the hydrogen film is utilized to transfer the CNT patterns and the filter paper is peeled to complete the transfer printing process. **Fig. 6b** shows the interdigitated CNT electrodes are transferred onto the hydrogel film. Note that the transferred electrode surfaces

remain clean and uniform while the feature size characterized by the gap between the comb fingers has a good resolution of ~100 μm. A wavy structure can be introduced to the carbon nanotube layer to improve the self-healing ability and flexibility *via* a pre-stretch-and-release method [59,74]. First, the hydrogel film is uniaxially pre-stretched for 130% to 150% of its original length before the CNT-electrode transfer process. Since the deformation of the hydrogel is in the elastic regime, the hydrogel can restore to its original length after the CNT transfer and subsequent release process (**Fig. 6c**). This introduced a compressive stress that leads to the wrinkling of CNT film (**Fig. S30**) and the formation of the wavy electrode (**Fig. 6d**).

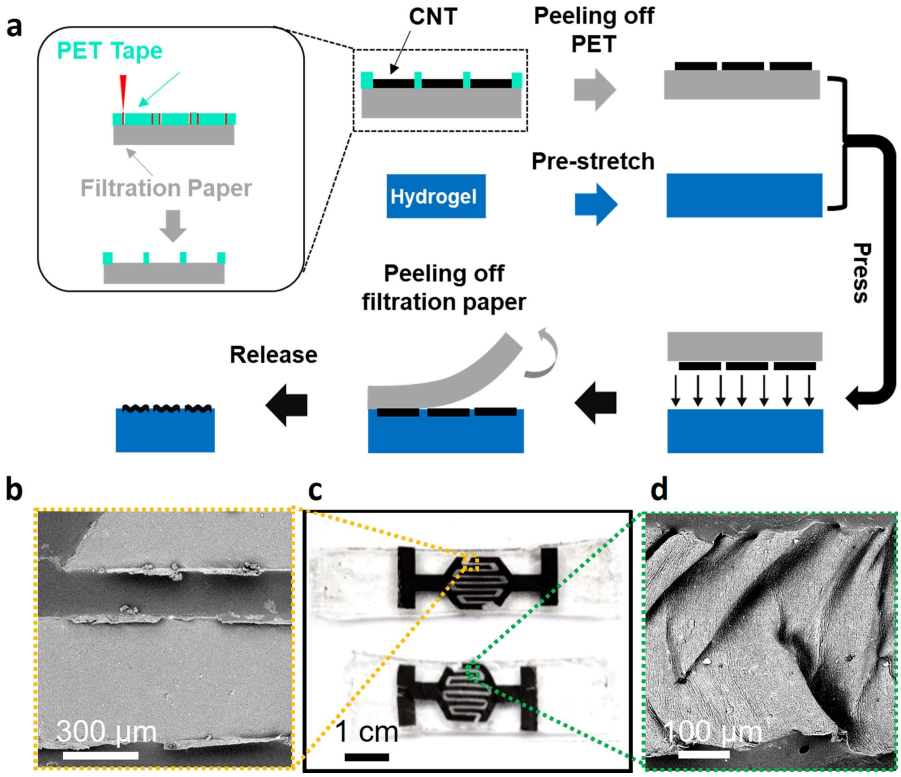

Fig. 6. (a) Schematic illustration of the transfer printing and pre-stretch-and-release process. **(b)** SEM image of the CNT electrode transferred onto a hydrogel film before the applied pre-strain is released. **(c)** Optical photo showing a pair of hexagon-shaped interdigitated CNT electrodes patterned on a hydrogel film before (top) and after (bottom) the strain release process. **(d)** SEM

image showing the wrinkled CNT electrode after the strain release process.

Self-healable micro-supercapacitor and humidity sensor

The excellent mechanical and electrical properties of the ionic skin in combination with the transfer-printing process can yield many different device structures. **Fig. 7a** shows a flexible supercapacitor with interdigitated electrodes, where the MA-LiCl hydrogel simultaneously serves as the substrate, electrolyte, and separator which can improve the energy density of the system and reduce the complexity of the fabrication process. Interdigitated electrodes are designed to be on the neutral plane of the device to alleviate the stress due to possible mechanical deformations and to maximize the contact area between the electrode and electrolyte by exposing the electrodes to both the top and bottom electrolyte. The wavy electrode structure also endows enhanced flexibility. As shown in **Fig. 7b**, cyclic voltammetry (CV) reveals that when folded 180-degree with a bending radius of ~1 mm, the device shows little performance changes (capacitance change <2%). The self-healing hydrogel in combination with the wavy electrode design (**Fig. S31**) yields the self-healable device. As demonstrated in **Fig. 7c**, a supercapacitor is completely cut through using a razor blade into two halves and subsequently reconnected together manually to allow for self-healing at room temperature. The dynamic nature of the reversible bonds helps the repeatable recovery at the same damaged areas (**Video 2**). As a result, the supercapacitor retains over 93% of initial capacitance over 10 cycles of repeated cutting and healing tests. The rate capability of the device is assessed with galvanostatic charge-discharge (GCD) and CV techniques. The supercapacitor exhibits near triangle-shaped GCD curves (**Fig. S32**) with a current density up to 2 mA/cm^2 and typical rectangular CV curves with a scan rate up to 500 mV/s (**Fig. 7d**), showing comparable performance to that of a similar device based on the conventional PVA/H_3PO_4 electrolyte (**Fig. S33**). The

dynamic stability of the hydrogel provides the device with robust and stable ion transport channels when exposed to air. As shown in **Fig. 7d**, 10,000 cycles are tested for the supercapacitor in the ambient environment and ~97.8% capacitance has been retained. Moreover, device performance over an extended hydrogel storage period has also been investigated. As shown in **Fig. 7e**, a prototype device fabricated with the hydrogel film stored under the ambient environment for 16 months exhibits nearly identical performance as compared to those made by a fresh hydrogel film, attributed to the moisture self-regulation of the hydrogel. Such capability also helps the device to survive in extreme conditions. As a demonstration, a prototype device has been placed to the subzero (-20 ℃) freezing condition for 24 h, under the 200 ℃ heating condition for 30 min, and under the vacuum drying condition overnight (~16 h). In each condition, the supercapacitor can recover more than 90% of its original capacitance once being placed back in the original ambient environment (**Fig. 7f**).

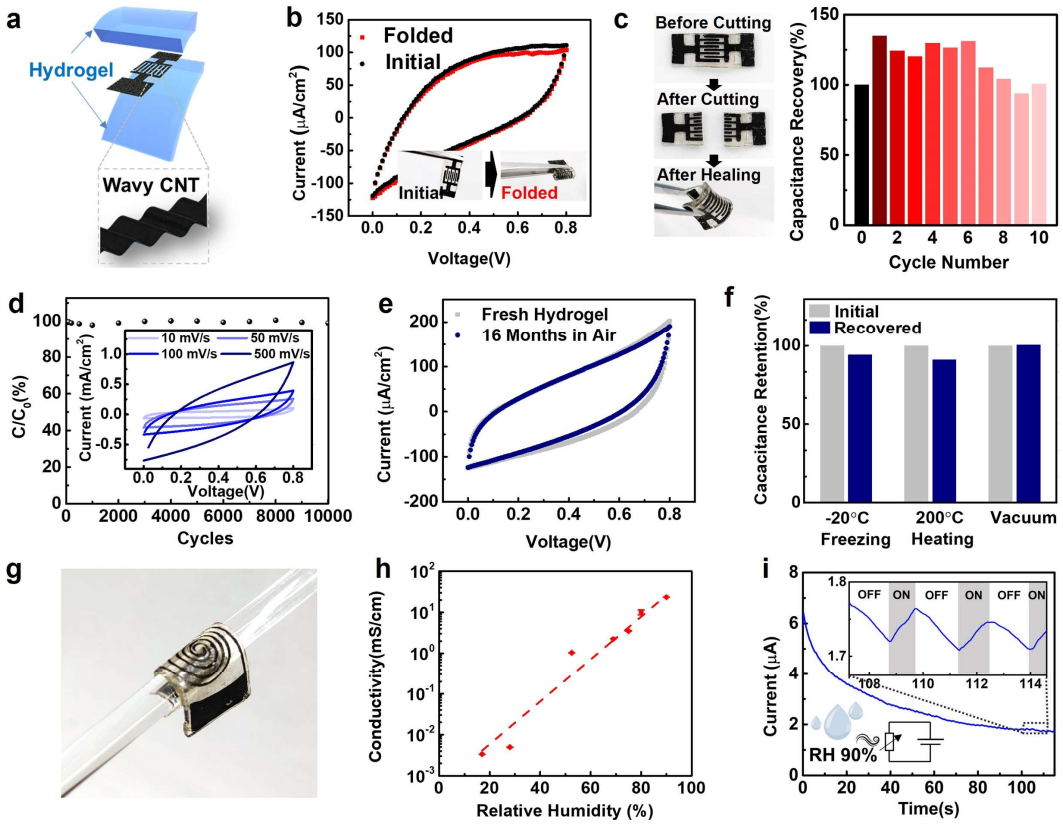

Fig. 7. (a) Schematic view of the transfer-printed supercapacitor with wavy CNT electrodes. **(b)** Optical images (inset) and CV curves of a supercapacitor before and after the folding process. All devices fabricated herein are based on MA-LiCl hydrogel (4 M LiCl, 0.06%). The scan rate of the CV curves is 100 mV/s. **(c)** Photos illustrating the self-healing process of the supercapacitors and its capacitance recovery results during the 10 cutting and healing cycles. **(d)** The capacitance retention performance of the device in the ambient environment (RH 69%) during 10,000 cycles at a scan rate of 100 mV/s. Inset: CV curves at different scan rate ranging from 10 mV/s to 500 mV/s. **(e)** Comparison of CV curves for supercapacitors fabricated from the fresh hydrogel film and the hydrogel film that has been stored in open air for 16 months. The scan rate is kept at 100 mV/s. **(f)** Capacitance recovery tests of supercapacitors after the exposures to low temperature (-20 °C, 1 day), high temperature (200 °C, 30 min), and vacuum (hundreds of mTorr, 16 hours) and

subsequently being transferred to the ambient environment (RH 69%). Time for the full recovery under the ambient environment is 48 h. **(g)** Photo illustrating the transfer-printed humidity sensor with spiral electrodes. **(h)** Ion conductivities of the LiCl hydrogel under a wide range of relative humidity levels (from 17% to 90%). **(i)** As-fabricated humidity sensor connected to the supercapacitor (pre-charged to 0.8 V) in series and the current changes are recorded as the room-temperature high humidity air (RH 90%) is intermittently applied to the sensor.

The transfer-printing process allows high versatility in the device design. **Fig. 7g** shows a flexible humidity sensor with the spiral-shape CNT electrodes and the hydrogel is utilized both as the active resistive sensing material and the substrate. The sensor exhibits a wide range of operational humidity levels (**Fig. 7h**) due to the excellent water retention capability of hydrogel. Using the MA-hydrogel ionic skin as the building block, a printed supercapacitor has been integrated with a printed hydrogel-based humidity sensor as a self-powered sensing system for potential application in human respiration monitoring. **Fig. 7i** shows the as-fabricated humidity sensor connected to the supercapacitor (pre-charged to 0.8 V) in series and the current changes are recorded at room temperature. As high humidity air (RH 90%) is intermittently applied to the sensor, the current response exhibits obvious rises due to transient humidity increases and the supercapacitor discharge continuously such that the base line of the output current consciously reduces as expected. In applications where a stability against humidity is desired, additional packing materials could be applied to prevent exchange of moistures due to daily humidity fluctuations[12,75]. Additionally, circuity design such as Wheatstone bridge or background subtraction algorithms could be implemented to compensate environmental effects in practical operations[76–78].

Conclusion

In summary, ultra-long ambient stability has been realized in self-healable ionic skins with self-regulated moisture levels. By introducing deliquescent salt for water uptake and zwitterionic moieties to dissociate the salt ions *via* anti-polyelectrolyte effects, mutually cohesive interactions between water, ions, and polymer backbone can be achieved as predicted by the MD simulations. As such, water vapor pressure in the system is significantly reduced to reach an equilibrium with the ambient humidity to achieve the self-regulation of moisture. A stretchable ionic conductor has been demonstrated to be fully functional in the ambient air for 16 months. After repeated exposures to various harsh conditions such as low and high temperature of -20 ℃ and 200 ℃, and vacuum, the hydrogel can replenish its water content by absorbing moistures from the ambient air and regain most of its original conductivity, stretchability and self-healing capability. In addition to promoting the dissociation of salt for augmented water retention capability, zwitterionic moieties synergistically couple with hydrogen-bond donor groups on the polymer backbone to provide dynamic bonds for autonomous self-healing. Other structures and materials can be facilely transfer-printed and/or integrated with the hydrogel to create various devices, such as self-healing flexible piezoelectret sensors, supercapacitors and humidity sensors as demonstrated in this work. The material design and fabrication strategies presented here could help the constructions of hybrid circuits of ions and electrons for applications in stretchable and wearable systems, including batteries, sensors, soft robotics, and other devices for human-machine interfaces.

Experimental Section

Ionic skin synthesis process. All chemicals were purchased from Sigma-Aldrich and used without further purification. MA-LiCl hydrogel was synthesized by dissolving 2-(methacryloyloxy)ethyl)

dimethyl-(3-sulfopropyl) ammonium hydroxide (MEDSAH, 0.75 g), acrylic acid (AA, 1.50 g), and LiCl (0.23 g for 2 M, 0.35 g for 3 M , 0.47 g for 4 M, 0.58 g for 5 M, 0.70 g for 6 M) into 2.75 mL of DI water to keep the mass ratio of MEDSAH to AA at 1:2. The initiator, ammonium persulphate (APS, 0.012 g) and specific amount of crosslinker (0.06 mol%, 0.03 mol%, 0.01 mol% 0.006 mol% to AA or no crosslinker), N,N-methylenebisacrylamide (MBAA) were then added accordingly to form the precursor solution. After complete dissolution, the solution was bubbled with N_2 for 10 minutes to deplete O_2 and the solution is poured into a polystyrene petri dish and heated at 50 ^oC for 24 h. MA, MA-EG and MA-NaCl hydrogels were synthesized in the identical procedure, except that no LiCl was added for the MA hydrogel and ethylene glycol (EG) and NaCl were used in MA-EG and MA-NaCl, respectively. The concentrations of EG and NaCl in water were both kept at 4 mol/L for consistency. For the ATR-FTIR characterizations, poly acrylic acid/LiCl (PAA-LiCl), poly(2-(methacryloyloxy)ethyl)dimethyl-(3-sulfopropyl) ammonium hydroxide) (PMEDSAH-LiCl) were synthesized in the same procedure without MEDSAH and AA, respectively.

Characterizations. SEM images of hydrogels and self-healing micro-supercapacitors were obtained using a tabletop SEM (Phenom Pro) at acceleration voltages of 5 kV and 10 kV, respectively. HATR-FTIR spectra were performed on Spectrum One FTIR Spectrometer (Perkin Elmer) with HATR sampling accessory, Raman spectra were measured on LabRAM Aramis Raman Microscope (Horiba) with an excitation wavelength of 532 nm and diffraction grating of 1800 g mm^{-1} grating, and UV-Vis spectra were collected on QualitySpec Pro UV-Vis Spectrometer (ASD Inc.). TGA was carried out on TGA 5500 (TA Instruments) in argon atmosphere from 25 ℃ to 600 ℃ with a ramp speed of 10 ℃/s. Differential scanning calorimetry (DSC Q1000, TA Instruments) was

used to study the low-temperature stability of hydrogels at a heating and cooling rate of 2 ℃ min^{-1} using Tzero Aluminum pans.

Mechanical and electrical characterization of hydrogel. Mechanical tensile tests were performed on strips of hydrogel samples using a tensile machine (Instron model 5544) at a stretch rate of 0.17 min^{-1} unless otherwise noted. The electrochemical impedances of the hydrogels were first measured using the electrochemical workstation (Gamry Reference 600) in a symmetric cell setup, where gold-coated PET films were used as inert electrodes. The ionic resistance of each sample was determined from the impedance with the phase shift near 0 degree. The measured resistance was converted to ionic conductivity:

$$\sigma = \frac{l}{R(t \cdot w)} = \frac{l}{RA}$$

Where l referred to the length of each hydrogel sample and A was the cross-section area (thickness times width) of each hydrogel. The area and thickness of each sample were measured and recorded before conducting each experiment. The resistance change of ionic skin with respect to mechanical stretch was measured by concurrently stretching the hydrogel using the tensile machine and measuring the ionic resistance of the hydrogel with the electrochemical workstation.

Water retention and cyclic moisture self-regulation tests. Water retention tests were conducted by placing the hydrogels into the ambient environments with humidity of RH 17%, 28%, 69%, and 75% at 25 ℃ for 7 consecutive days. The weight at each humidity level was measured each day to find the stable weight values at each humidity level. The total mass retention ratio of each hydrogel was calculated by utilizing the following equation:

$$weight\ retention\ (\%)\ = w/w_0 * 100\%$$

Where w_0 and w refer to retained weight of each hydrogel on day 0 (before conducting experiments) and the corresponding testing day, respectively. The ionic conductivities of each hydrogel at the humidity of RH 17%, 28%, 69%, and 75% were also measured for 7 consecutive days to find the stable conductivity values at each humidity level. Prior to the experiment, as-prepared hydrogel samples were stored and equilibrated at RH 80%, and their initial ion conductivities and masses were recorded before being transferred to chambers at different humidity levels. The cyclic moisture self-regulation test was conducted by alternatively putting hydrogels into two distinct humidity environments at RH 17% and 69% for 6 cycles and the stabilized ion conductivity values were recorded during each cycle.

Fabrication and signal acquisition of self-powered transparent piezoelectret sensor. The proposed sensor was fabricated with the following steps. First, a dielectric elastomer (VHB 4905, 3M) film was perforated using a hole puncher (hole diameter of 6 mm, Kucaa, China) and sandwiched between two layers of 12.7 μm-thick fluorinated ethylene propylene (FEP) films. Second, a MA-LiCl hydrogel film (thickness of 1 mm) and a layer of unperforated dielectric elastomer (VHB 4905, 3M) were applied on top of the FEP-VHB-FEP sandwich structure to form the sensor, where the MA-LiCl ionic skin serves as the transparent soft electrode. No bonding reagent was used for the assembly of the device due to the self-adhesion properties of both MA-LiCl hydrogel and VHB elastomer. Third, the device was corona-charged following a previously reported procedure[75] (-18 kV, 30 mins), such that the air in between FEP films was ionized for piezoelectricity-like performances. During signal acquisitions, the sensor was conformally attached using a band-aid belt (for muscle movement measurement) or an air-pumped wristband (for pulse

measurement) on the volunteer's arm, which was grounded *via* a gel electrode (Red Dot 2560, 3M). The generated analog signal was collected by a low-noise current preamplifier (Model SR570) at a low pass frequency of 30 Hz. The analog signals were then transformed to digital signals at a sampling rate of 100 points per second *via* a digital I/O (NI-USB-6341) and saved to a local computer.

Fabrication and characterization of ionic skin-based supercapacitor and humidity sensor. The fabrication of wavy CNT electrodes on hydrogel was done by first patterning CNT on a nylon membrane filter with a diameter of 47 mm and pore size of 0.2 μm (364-2612-OEM EZFlow, Foxx Life Sciences) *via* a reported method[73]. Specifically, a layer of 50 μm-thick adhesive polyethylene terephthalate (PET, Gizmo Dorks) was adhered to the membrane filter to form a bilayer. Patterns were then cut out by a mechanical cutting machine (Silhouette, CAMEO 3) on the upper PET layer, which then served as the shadow mask for the filtration of 5 mL aqueous dispersion of carbon nanotubes (AP-SWNT, Carbon Solutions Inc.) with a CNT loading of 0.33 mg mL^{-1}. Herein, the CNT aqueous dispersion was typically prepared by adding 50 mg of CNT and 200 mg of sodium dodecylbenzene sulfonate (SDBS) into 150 mL of DI water and dispersed using a tip horn sonicator (Q500, Qsonica). Meanwhile, a strip of MA-LiCl hydrogel was cut into a desired size and pre-stretched uniaxially. The pre-stretched hydrogel was then pressed onto the filter membrane to allow for close contact with the pattern CNT. Thereafter, the filter membrane was peeled off to transfer the CNT patterns onto the hydrogel. Finally, the pre-strain was released from the hydrogel to induce wavy structures on CNT electrodes. Another layer of MA-hydrogel was pressed on top of the interdigitated electrodes to form the supercapacitor, while the CNT electrodes for the humidity sensor were left exposed to air. The performance of the assembled

supercapacitor was measured on the electrochemical workstation (*Gamry Reference 600*) *via* CV, GCD, and EIS tests. CV and GCD measurements were carried out within the voltage from 0 to 0.8 V. The real and imaginary parts of impedance (Z and Z') were recorded during EIS tests, over a frequency range between 0.1 Hz and 10^5 Hz. The self-powered system for humidity detection was constructed by connecting an as-fabricated humidity sensor in series with a supercapacitor (pre-charged to 0.8V) and the current change through the circuit were recorded using the electrochemical workstation. Temperature changes induced by breathing are monitored by a commercial thermistor-based temperature sensor (Sensirion AG SHT4X). MA-LiCl hydrogel is either exposed to ambient air or completely encapsulated by VHB tape (VHB 4905, 3M) during the measurement of ionic resistance change at varying temperatures. Ionic resistance is measured with electrochemical workstation using the method described above in this section.

Competing interests: The authors declare that they have no competing interests.

Acknowledgments. †Peisheng He, Yu Long and Chao Fang contributed equally to this work. This project is supported in part by the Berkeley Sensor and Actuator Center and the Science and Technology Development Fund, Macau SAR (FDCT) (File No. 0059/2021/AFJ, 0040/2021/A1). Work was performed in part at the Biomolecular Nanotechnology Centre (BNC) laboratory and Marvell Nanofabrication Laboratory at the University of California, Berkeley and at the Molecular Foundry, Lawrence Berkeley National Laboratory. Work at the Molecular Foundry was supported by the Office of Science, Office of Basic Energy Sciences, of the U.S. Department of Energy under Contract No. DE-AC02-05CH11231.

Appendix A. Supplementary materials

Supplementary data associated with this article can be found in the online version at……

References

[1] Y. Zhao, Y. Zhang, H. Sun, X. Dong, J. Cao, L. Wang, Y. Xu, J. Ren, Y. Hwang, I. H. Son, X. Huang, Y. Wang, H. Peng, A Self-Healing Aqueous Lithium-Ion Battery. Angew. Chem. Int. Ed. 55 (2016) 14384–14388.
https://doi.org/10.1002/ANIE.201607951.

[2] R. Narayan, C. Laberty-Robert, J. Pelta, J. M. Tarascon, R. Dominko, Self-Healing: An Emerging Technology for Next-Generation Smart Batteries. Adv. Energy Mater. 12 (2022) 2102652.
https://doi.org/10.1002/AENM.202102652.

[3] S. Huang, F. Wan, S. Bi, J. Zhu, Z. Niu, J. Chen, A Self-Healing Integrated All-in-One Zinc-Ion Battery. Angew. Chem. Int. Ed. 58 (2019) 4313–4317.
https://doi.org/10.1002/ANGE.201814653.

[4] Y. Huang, M. Zhong, Y. Huang, M. Zhu, Z. Pei, Z. Wang, Q. Xue, X. Xie, C. Zhi, A Self-Healable and Highly Stretchable Supercapacitor Based on a Dual Crosslinked Polyelectrolyte. Nat. Commun. 6 (2015) 10310.
https://doi.org/10.1038/ncomms10310.

[5] H. Li, T. Lv, H. Sun, G. Qian, N. Li, Y. Yao, T. Chen, Ultrastretchable and Superior Healable Supercapacitors Based on a Double Cross-Linked Hydrogel Electrolyte. Nat. Commun. 10 (2019) 536.
https://doi.org/10.1038/s41467-019-08320-z.

[6] N. Lu, R. Na, L. Li, C. Zhang, Z. Chen, S. Zhang, J. Luan, G. Wang, Rational Design of Antifreezing Organohydrogel Electrolytes for Flexible Supercapacitors. ACS Appl. Energy Mater. 3 (2020) 1944–1951. https://doi.org/10.1021/acsaem.9b02379.

[7] J. Huang, S. Peng, J. Gu, G. Chen, J. Gao, J. Zhang, L. Hou, X. Yang, X. Jiang, L. Guan, Self-Powered Integrated System of a Strain Sensor and Flexible All-Solid-State Supercapacitor by Using a High Performance Ionic Organohydrogel. Mater. Horiz. 7 (2020) 2085–2096. https://doi.org/10.1039/d0mh00100g.

[8] J. Y. Sun, C. Keplinger, G. M. Whitesides, Z. Suo, Ionic Skin. Adv. Mater. 26 (2014) 7608–7614. https://doi.org/10.1002/adma.201403441.

[9] C. Keplinger, J. Y. Sun, C. C. Foo, P. Rothemund, G. M. Whitesides, Z. Suo, Stretchable, Transparent, Ionic Conductors. Science 341 (2013) 984–987. https://doi.org/10.1126/SCIENCE.1240228.

[10] X. Qiu, J. Liu, B. Zhou, X. Zhang, X. Qiu, J. Liu, B. Zhou, X. Zhang, Bioinspired Bimodal Mechanosensors with Real-Time, Visualized Information Display for Intelligent Control, Adv. Funct. Mater. 33 (2023) 2300321. https://doi.org/10.1002/ADFM.202300321.

[11] J. Yin, N. Liu, P. Jia, Z. Ren, Q. Zhang, W. Lu, Q. Yao, M. Deng, Y. Gao, MXene-enhanced environmentally stable organohydrogel ionic diode toward harvesting ultralow-frequency mechanical energy and moisture energy, SusMat. 3 (2023) 859–876. https://doi.org/10.1002/SUS2.169.

[12] C. Yang, Z. Suo, Hydrogel Ionotronics. Nat. Rev. Mater. 3 (2018) 125–142. https://doi.org/10.1038/s41578-018-0018-7.

[13] Y. Cao, Y. J. Tan, S. Li, W. W. Lee, H. Guo, Y. Cai, C. Wang, B. C. K. Tee, Self-Healing Electronic Skins for Aquatic Environments. Nat. Electron. 2 (2019) 75–82. https://doi.org/10.1038/s41928-019-0206-5.

[14] Z. Lei, P. Wu, A Supramolecular Biomimetic Skin Combining a Wide Spectrum of Mechanical Properties and Multiple Sensory Capabilities. Nat. Commun. 9 (2018) 1134. https://doi.org/10.1038/s41467-018-03456-w.

[15] W. Xie, J. Duan, H. Wang, J. Li, R. Liu, B. Yu, S. Liu, J. Zhou, Ultra-Stretchable, Bio-Inspired Ionic Skins That Work Stably in Various Harsh Environments. J. Mater. Chem. A 6 (2018) 24114–24119. https://doi.org/10.1039/c8ta09206k.

[16] L. Han, H. Zhang, H.-Y. Yu, Z. Ouyang, J. Yao, I. Krucinska, D. Kim, K. C. Tam, Highly Sensitive Self-Healable Strain Biosensors Based on Robust Transparent Conductive Nanocellulose Nanocomposites: Relationship between Percolated Network and Sensing Mechanism. Biosens. Bioelectron. 191 (2021) 113467. https://doi.org/10.1016/J.BIOS.2021.113467.

[17] J. Kang, J. B. H. Tok, Z. Bao, Self-Healing Soft Electronics. Nat. Electron. 2 (2019) 144–150. https://doi.org/10.1038/s41928-019-0235-0.

[18] L. Shi, T. Zhu, G. Gao, X. Zhang, W. Wei, S. Liu, S. Ding, Highly Stretchable and Transparent Ionic Conducting Elastomers. Nat. Commun. 9 (2018) 2630. https://doi.org/10.1038/s41467-018-05165-w.

[19] N. Wang, X. Yang, X. Zhang, Ultrarobust subzero healable materials enabled by polyphenol nano-assemblies, Nat. Commun. 14 (2023) 814. https://doi.org/10.1038/s41467-023-36461-9.

[20] Y. Bai, B. Chen, F. Xiang, J. Zhou, H. Wang, Z. Suo, Transparent Hydrogel with Enhanced Water Retention Capacity by Introducing Highly Hydratable Salt. Appl. Phys. Lett. 105 (2014) 151903.
https://doi.org/10.1063/1.4898189.

[21] C. Wang, M. Zhu, H.-Y. Yu, S. Y. H. Abdalkarim, Z. Ouyang, J. Zhu, J. Yao, Multifunctional Biosensors Made with Self-Healable Silk Fibroin Imitating Skin. ACS Appl. Mater. Interfaces 13 (2021) 33371–33382.
https://doi.org/10.1021/acsami.1c08568.

[22] S. Kondaveeti, G. Choi, S.C. Veerla, S. Kim, J. Kim, H.J. Lee, U. Kuzhiumparambil, P.J. Ralph, J. Yeo, H.E. Jeong, Mussel-inspired resilient hydrogels with strong skin adhesion and high-sensitivity for wearable device, Nano Converg. 11 (2024) 12.
https://doi.org/10.1186/s40580-024-00419-4.

[23] B. Chen, J. J. Lu, C. H. Yang, J. H. Yang, J. Zhou, Y. M. Chen, Z. Suo, Highly Stretchable and Transparent Ionogels as Nonvolatile Conductors for Dielectric Elastomer Transducers. ACS Appl. Mater. Interfaces 6 (2014) 7840–7845.
https://doi.org/10.1021/am501130t.

[24] B. Zhao, J. Yan, F. Long, W. Qiu, G. Meng, Z. Zeng, H. Huang, H. Wang, N. Lin, X.Y. Liu, Bioinspired Conductive Enhanced Polyurethane Ionic Skin as Reliable Multifunctional Sensors, Adv. Sci. 10 (2023) 2300857.
https://doi.org/10.1002/ADVS.202300857.

[25] H. Lee, S. Lee, W. Lee, T. Yokota, K. Fukuda, T. Someya, Ultrathin Organic Electrochemical Transistor with Nonvolatile and Thin Gel Electrolyte for Long-Term Electrophysiological Monitoring. Adv. Funct. Mater. 29 (2019) 1906982. https://doi.org/10.1002/adfm.201906982.

[26] Z. Lei, P. Wu, A Highly Transparent and Ultra-Stretchable Conductor with Stable

Conductivity during Large Deformation. Nat. Commun. 10 (2019) 3429. https://doi.org/10.1038/s41467-019-11364-w.

[27] Y. M. Kim, H. C. Moon, Ionoskins: Nonvolatile, Highly Transparent, Ultrastretchable Ionic Sensory Platforms for Wearable Electronics. Adv. Funct. Mater. 30 (2020) 1907290. https://doi.org/10.1002/adfm.201907290.

[28] Y. Ye, H. Oguzlu, J. Zhu, P. Zhu, P. Yang, Y. Zhu, Z. Wan, O.J. Rojas, F. Jiang, Ultrastretchable Ionogel with Extreme Environmental Resilience through Controlled Hydration Interactions, Adv. Funct. Mater. 33 (2023) 2209787. https://doi.org/10.1002/ADFM.202209787.

[29] J. Lee, M. W. M. Tan, K. Parida, G. Thangavel, S. A. Park, T. Park, P. S. Lee, Water-Processable, Stretchable, Self-Healable, Thermally Stable, and Transparent Ionic Conductors for Actuators and Sensors. Adv. Mater. 32 (2020) 1906679. https://doi.org/10.1002/adma.201906679.

[30] J. Wu, Z. Wu, H. Xu, Q. Wu, C. Liu, B. R. Yang, X. Gui, X. Xie, K. Tao, Y. Shen, J. Miao, L. K. Norford, An Intrinsically Stretchable Humidity Sensor Based on Anti-Drying, Self-Healing and Transparent Organohydrogels. Mater. Horiz. 6 (2019) 595–603. https://doi.org/10.1039/c8mh01160e.

[31] J. Song, S. Chen, L. Sun, Y. Guo, L. Zhang, S. Wang, H. Xuan, Q. Guan, Z. You, Mechanically and Electronically Robust Transparent Organohydrogel Fibers. Adv. Mater. 32 (2020) 1906994. https://doi.org/10.1002/adma.201906994.

[32] B. Ying, R. Z. Chen, R. Zuo, J. Li, X. Liu, An Anti-Freezing, Ambient-Stable and Highly Stretchable Ionic Skin with Strong Surface Adhesion for Wearable Sensing and Soft Robotics. Adv. Funct. Mater. 31 (2021) 2104665.

https://doi.org/10.1002/adfm.202104665.

[33] A. E. Marcinkowsky, H. O. Phillips, K. A. Kraus, Properties of Organic-Water Mixtures. VII. Self-Diffusion Coefficients of Na+ in Ethylene Glycol-Water and Glycerol-Water Mixtures at 25°. J. Phys. Chem. 72 (1968) 1201–1203.

https://doi.org/10.1021/j100850a021.

[34] Y. Jian, S. Handschuh-Wang, J. Zhang, W. Lu, X. Zhou, T. Chen, Biomimetic Anti-Freezing Polymeric Hydrogels: Keeping Soft-Wet Materials Active in Cold Environments. Mater. Horiz. 8 (2021) 351–369.

https://doi.org/10.1039/d0mh01029d.

[35] X. Sui, H. Guo, P. Chen, Y. Zhu, C. Wen, Y. Gao, J. Yang, X. Zhang, L. Zhang, Zwitterionic Osmolyte-Based Hydrogels with Antifreezing Property, High Conductivity, and Stable Flexibility at Subzero Temperature. Adv. Funct. Mater. 30 (2020) 1907986.

https://doi.org/10.1002/adfm.201907986.

[36] M. Rusdi, Y. Moroi, H. Nakahara, O. Shibata, Evaporation from Water-Ethylene Glycol Liquid Mixture. Langmuir 21 (2005) 7308–7310.

https://doi.org/10.1021/la040134g.

[37] H. K. Cammenga, F. W. Schulze, W. Theuerl, Vapor Pressure and Evaporation Coefficient of Glycerol. J Chem. Eng. Data 22 (1977) 131–134.

https://doi.org/10.1021/je60073a004.

[38] H. Lu, W. Shi, J. H. Zhang, A. C. Chen, W. Guan, C. Lei, J. R. Greer, S. V Boriskina, G. Yu, Tailoring the Desorption Behavior of Hygroscopic Gels for Atmospheric Water Harvesting in Arid Climates. Adv. Mater. 34 (2022) 2205344.

https://doi.org/10.1002/ADMA.202205344.

[39] Y. Guo, W. Guan, C. Lei, H. Lu, W. Shi, G. Yu, Scalable Super Hygroscopic Polymer Films for Sustainable Moisture Harvesting in Arid Environments. Nat. Commun. 13 (2022) 2761. https://doi.org/10.1038/s41467-022-30505-2.

[40] G. Graeber, C. D. Díaz-Marín, L. C. Gaugler, Y. Zhong, B. El Fil, X. Liu, E. N. Wang, Extreme Water Uptake of Hygroscopic Hydrogels through Maximized Swelling-Induced Salt Loading. Adv. Mater. 2211783 (2023). https://doi.org/10.1002/ADMA.202211783.

[41] Z. Wu, W. Shi, H. Ding, B. Zhong, W. Huang, Y. Zhou, X. Gui, X. Xie, J. Wu, Ultrastable, Stretchable, Highly Conductive and Transparent Hydrogels Enabled by Salt-Percolation for High-Performance Temperature and Strain Sensing. J. Mater. Chem. C 9 (2021) 13668–13679. https://doi.org/10.1039/d1tc02506f.

[42] X. F. Zhang, X. Ma, T. Hou, K. Guo, J. Yin, Z. Wang, L. Shu, M. He, J. Yao, Inorganic Salts Induce Thermally Reversible and Anti-Freezing Cellulose Hydrogels. Angew. Chem. Int. Ed. 58 (2019) 7366–7370. https://doi.org/10.1002/anie.201902578.

[43] W. Ge, S. Cao, Y. Yang, O. J. Rojas, X. Wang, Nanocellulose/LiCl Systems Enable Conductive and Stretchable Electrolyte Hydrogels with Tolerance to Dehydration and Extreme Cold Conditions. Chem. Eng. J. 408 (2021) 127306. https://doi.org/10.1016/j.cej.2020.127306.

[44] Y. Zhang, S. Furyk, D. E. Bergbreiter, P. S. Cremer, Specific Ion Effects on the Water Solubility of Macromolecules: PNIPAM and the Hofmeister Series. J. Am. Chem. Soc. 127 (2005) 14505–14510. https://doi.org/10.1021/JA0546424.

[45] M. Hua, S. Wu, Y. Ma, Y. Zhao, Z. Chen, I. Frenkel, J. Strzalka, H. Zhou, X. Zhu, X. He,

Strong Tough Hydrogels via the Synergy of Freeze-Casting and Salting Out. Nature 590 (2021) 594–599.
https://doi.org/10.1038/s41586-021-03212-z.

[46] S. Xiao, Y. Zhang, M. Shen, F. Chen, P. Fan, M. Zhong, B. Ren, J. Yang, J. Zheng, Structural Dependence of Salt-Responsive Polyzwitterionic Brushes with an Anti-Polyelectrolyte Effect. Langmuir 34 (2018) 97–105.
https://doi.org/10.1021/acs.langmuir.7b03667.

[47] J. F. Young, Humidity Control in the Laboratory Using Salt Solutions-a Review. J. Appl. Chem. 17 (2007) 241–245.
https://doi.org/10.1002/jctb.5010170901.

[48] H. G. Leopold, J. Johnston, The Vapor Pressure of the Saturated Aqueous Solutions of Certain Salts. J. Am. Chem. Soc. 49 (1927) 1974–1988.
https://doi.org/10.1021/ja01407a019.

[49] W. Shi, W. Guan, C. Lei, G. Yu, Sorbents for Atmospheric Water Harvesting: From Design Principles to Applications, Angew. Chem. Int. Ed. 61 (2022) e202211267.
https://doi.org/10.1002/ANIE.202211267.

[50] X. Zang, C. Jian, T. Zhu, Z. Fan, W. Wang, M. Wei, B. Li, M. Follmar Diaz, P. Ashby, Z. Lu, Y. Chu, Z. Wang, X. Ding, Y. Xie, J. Chen, J. N. Hohman, M. Sanghadasa, J. C. Grossman, L. Lin, Laser-Sculptured Ultrathin Transition Metal Carbide Layers for Energy Storage and Energy Harvesting Applications. Nat. Commun. 10 (2019) 3112.
https://doi.org/10.1038/s41467-019-10999-z.

[51] F. Chen, D. Zhou, J. Wang, T. Li, X. Zhou, T. Gan, S. Handschuh-Wang, X. Zhou, Rational Fabrication of Anti-Freezing, Non-Drying Tough Organohydrogels by One-Pot Solvent Displacement. Angew. Chem. Int. Ed. 130 (2018) 6678–6681.

https://doi.org/10.1002/ange.201803366.

[52] K. Kabiri, H. Mirzadeh, M. J. Zohuriaan-Mehr, Chitosan Modified MMT-Poly(AMPS) Nanocomposite Hydrogel: Heating Effect on Swelling and Rheological Behavior. J. Appl. Polym. Sci. 116 (2010) 2548–2556.

https://doi.org/10.1002/APP.31727.

[53] K. Kabiri, H. Mirzadeh, M. J. Zohuriaan-Mehr, Undesirable Effects of Heating on Hydrogels. J. Appl. Polym. Sci. 110 (2008) 3420–3430.

https://doi.org/10.1002/APP.28148.

[54] X. Jiang, C. Wang, Q. Han, Molecular Dynamic Simulation on the State of Water in Poly(Vinyl Alcohol) Hydrogel. Comput. Theor. Chem. 1102 (2017) 15–21.

https://doi.org/10.1016/j.comptc.2016.12.041.

[55] Y. Sekine, T. Ikeda-Fukazawa, Structural Changes of Water in a Hydrogel during Dehydration. J. Chem. Phys. 130 (2009) 034501.

https://doi.org/10.1063/1.3058616.

[56] Z. H. Ping, Q. T. Nguyen, S. M. Chen, J. Q. Zhou, Y. D. Ding, States of Water in Different Hydrophilic Polymers - DSC and FTIR Studies. Polymer (Guildf) 42 (2001) 8461–8467.

https://doi.org/10.1016/S0032-3861(01)00358-5.

[57] M. S. Jhon, J. D. Andrade, Water and Hydrogels. J. Biomed. Mater. Res. 7 (1973) 509–522.

https://doi.org/10.1002/jbm.820070604.

[58] Y. Liu, X. Liu, B. Duan, Z. Yu, T. Cheng, L. Yu, L. Liu, K. Liu, Polymer-Water Interaction Enabled Intelligent Moisture Regulation in Hydrogels. J. Phys. Chem. Lett. 12 (2021) 2587–2592.

https://doi.org/10.1021/acs.jpclett.1c00034.

[59] M. R. Conde, Properties of Aqueous Solutions of Lithium and Calcium Chlorides:

Formulations for Use in Air Conditioning Equipment Design. Int. J. Therm. Sci. 43 (2004) 367–382.
https://doi.org/10.1016/j.ijthermalsci.2003.09.003.

[60] H. Kamata, Y. Akagi, Y. Kayasuga-Kariya, U. Il Chung, T. Sakai, "Nonswellable" Hydrogel without Mechanical Hysteresis. Science 343 (2014) 873–875.
https://doi.org/10.1126/SCIENCE.1247811.

[61] W. Zhang, X. Liu, J. Wang, J. Tang, J. Hu, T. Lu, Z. Suo, Fatigue of Double-Network Hydrogels. Eng. Fract. Mech. 187 (2018) 74–93.
https://doi.org/10.1016/j.engfracmech.2017.10.018.

[62] H. R. Brown, A Model of the Fracture of Double Network Gels. Macromolecules 40 (2007) 3815–3818.
https://doi.org/10.1021/ma062642y.

[63] A. Phadke, C. Zhang, B. Arman, C. C. Hsu, R. A. Mashelkar, A. K. Lele, M. J. Tauber, G. Arya, S. Varghese, Rapid Self-Healing Hydrogels. Proc. Natl. Acad. Sci. U. S. A. 109 (2012) 4383–4388.
https://doi.org/10.1073/PNAS.1201122109

[64] J. Dong, Y. Ozaki, K. Nakashima, Infrared, Raman, and near-infrared spectroscopic evidence for the coexistence of various hydrogen-bond forms in poly(acrylic acid), Macromolecules 30 (1997) 1111–1117.
https://doi.org/10.1021/ma960693x.

[65] J. Yang, Z. Xu, J. Wang, L. Gai, X. Ji, H. Jiang, L. Liu, Antifreezing Zwitterionic Hydrogel Electrolyte with High Conductivity of 12.6 mS cm−1 at −40 °C through Hydrated Lithium Ion Hopping Migration, Adv. Funct. Mater. 31 (2021) 2009438.
https://doi.org/10.1002/ADFM.202009438.

[66] T. Xu, L. Zhang, B. Song, X. Bai, Z. Huang, X. Bu, T. Chen, H. Fu, P. Guo, High-strain sensitive zwitterionic hydrogels with swelling-resistant and controllable rehydration for sustainable wearable sensor, J. Colloid Interface Sci. 620 (2022) 14–23. https://doi.org/10.1016/j.jcis.2022.03.125.

[67] R. Barbucci, A. Magnani, M. Consumi, Swelling Behavior of Carboxymethylcellulose Hydrogels in Relation to Cross-Linking, PH, and Charge Density. Macromolecules 33 (2000) 7475–7480. https://doi.org/10.1021/ma0007029.

[68] T. Sekitani, Y. Noguchi, K. Hata, T. Fukushima, T. Aida, T. Someya, A Rubberlike Stretchable Active Matrix Using Elastic Conductors. Science 321 (2008) 1468–1472. https://doi.org/10.1126/science.1160309.

[69] M. D. Dickey, Stretchable and Soft Electronics Using Liquid Metals. Adv. Mater. 29 (2017) 1606425. https://doi.org/10.1002/adma.201606425.

[70] C. S. Boland, U. Khan, G. Ryan, S. Barwich, R. Charifou, A. Harvey, C. Backes, Z. Li, M. S. Ferreira, M. E. Möbius, R. J. Young, J. N. Coleman, Sensitive Electromechanical Sensors Using Viscoelastic Graphene-Polymer Nanocomposites. Science 354 (2016) 1257–1260. https://doi.org/10.1126/science.aag2879.

[71] J. Zhong, Y. Ma, Y. Song, Q. Zhong, Y. Chu, I. Karakurt, D. B. Bogy, L. Lin, A Flexible Piezoelectret Actuator/Sensor Patch for Mechanical Human Machine Interfaces. ACS Nano 13 (2019) 7107–7116. https://doi.org/10.1021/acsnano.9b02437.

[72] F. Fan, J. Szpunar, Characterization of Viscoelasticity and Self-Healing Ability of VHB 4910. Macromol. Mater. Eng. 300 (2015) 99–106.

https://doi.org/10.1002/mame.201400122.

[73] R. Xu, P. He, G. Lan, K. Behrouzi, Y. Peng, D. Wang, T. Jiang, A. Lee, Y. Long, L. Lin, Facile Fabrication of Multilayer Stretchable Electronics via a Two-Mode Mechanical Cutting Process. ACS Nano 16 (2022) 1533–1546.

https://doi.org/10.1021/acsnano.1c10011.

[74] S. Yan, G. Zhang, H. Jiang, F. Li, L. Zhang, Y. Xia, Z. Wang, Y. Wu, H. Li, Highly Stretchable Room-Temperature Self-Healing Conductors Based on Wrinkled Graphene Films for Flexible Electronics. ACS Appl. Mater. Interfaces 11 (2019) 10736–10744.

https://doi.org/10.1021/acsami.9b00274.

[75] P. Le Floch, X. Yao, Q. Liu, Z. Wang, G. Nian, Y. Sun, L. Jia, Z. Suo, Wearable and Washable Conductors for Active Textiles, ACS Appl. Mater. Interfaces 9 (2017) 25542–25552.

https://doi.org/10.1021/acsami.7b07361.

[76] Y. Park, H. Luan, K. Kwon, T.S. Chung, S. Oh, J.Y. Yoo, G. Chung, J. Kim, S. Kim, S.S. Kwak, J. Choi, H.P. Phan, S. Yoo, H. Jeong, J. Shin, S.M. Won, H.J. Yoon, Y.H. Jung, J.A. Rogers, Soft, full Wheatstone bridge 3D pressure sensors for cardiovascular monitoring, npj Flex. Electron. 8 (2024) 6.

https://doi.org/10.1038/s41528-024-00294-3.

[77] A. Somov, A. Baranov, A. Suchkov, A. Karelin, S. Mironov, E. Karpova, Improving interoperability of catalytic sensors, Sens. Actuators, B. 221 (2015) 1156–1161.

https://doi.org/10.1016/j.snb.2015.07.082.

[78] A.M. Ruminski, M.M. Moore, M.J. Sailor, Humidity-compensating sensor for volatile organic compounds using stacked porous silicon photonic crystals, Adv. Funct. Mater. 18 (2008) 3418–3426.

https://doi.org/10.1002/ADFM.200701494.